Applied Catalysis B: Environmental 312 (2022) 121383

Contents lists available at ScienceDirect

Applied Catalysis B: Environmental

journal homepage: www.elsevier.com/locate/apcatb

Rational synthesis of ruthenium-based metallo-supramolecular polymers as heterogeneous catalysts for catalytic transfer hydrogenation of carbonyl compounds

Zi-Jie Gong [a,b], Yemineni S.L.V. Narayana [c], Yen-Chun Lin [a], Wei-Hsiang Huang [d], Wei-Nien Su [d], Yi-Pei Li [a], Masayoshi Higuchi [c,*], Wen-Yueh Yu [a,b,**]

[a] Department of Chemical Engineering, National Taiwan University, Taipei 10617, Taiwan
[b] Advanced Research Center for Green Materials Science and Technology, Taipei 10617, Taiwan
[c] Electronic Functional Macromolecules Group, Research Center for Functional Materials, National Institute for Materials Science, Tsukuba, Ibaraki 305-0044, Japan
[d] Graduate Institute of Applied Science and Technology, National Taiwan University of Science and Technology, Taipei 10607, Taiwan

ARTICLE INFO

Keywords:
Metallo-supramolecular polymer
Heterogeneous catalyst
Catalytic transfer hydrogenation
Carbonyl reduction

ABSTRACT

Ruthenium-based metallo-supramolecular polymers (Ru-MSPs) were synthesized by complexing Ru ions with 1,4-bis(1,10-phenanthrolin-5-yl)benzene ligands for heterogeneously catalytic transfer hydrogenation of carbonyl compounds with formate. The degree of polymerization and the local environment of Ru atoms in Ru-MSP were tailored by tuning the ligand/metal ratio and the synthesis temperature/period. The coordinatively-unsaturated Ru atoms are identified as the active centers in Ru-MSP for carbonyl reduction. Ru-MSP is much more active than Ru-based counterparts including its monomeric analogue, which is attributed to (1) the higher electron density in Ru atoms that facilitates the selective dehydrogenation of formate *via* C-H dissociation, and (2) the lower LUMO of ligand moieties that activates the carbonyl oxygen *via* Lewis acid-base interactions. Furthermore, Ru-MSP displays high reusability and capability of catalyzing a wide scope of carbonyl compounds. These findings demonstrate that the rationally-designed polymerization is a promising approach to heterogenize the catalytically active metal complexes with enhanced performance.

1. Introduction

Catalytic reduction plays an important role in many industrial processes, particularly for the sustainable transformations of oxygen-rich lignocellulosic biomass into value-added products *via* carbonyl reduction [1,2]. Using liquid hydrogen donors (*e.g.*, formic acid, and isopropyl alcohol), the catalytic transfer hydrogenation (CTH) has emerged as a promising strategy to reduce the molecules in an environmental-friendly manner [3–5]. Compared to the molecular hydrogen, the liquid hydrogen donors used in CTH reactions are generally easier to tackle and show favorable product selectivity due to the controllable reduction ability. Among liquid hydrogen donors, formic acid is appealing [6,7] as it could generally dehydrogenate under relatively mild conditions due to a low activation barrier [6,8–10], while formate is often instead employed in order to circumvent the potential corrosion issue of formic acid [11–13].

Homogeneous metal complexes such as chiral complexes [11], half-sandwich complexes [13], and pincer-type complexes [14–16] have been widely utilized as homogeneous catalysts for the CTH reactions. Despite the exceptional catalytic performance, the relatively poor recyclability due to inherent homogeneity remains a significant barrier that limits the practical applications of homogeneous metal complex catalysts. To address this issue, the common heterogenization approach is to immobilize the metal complexes onto a solid support such as carbon, Al_2O_3, and SiO_2 [17–21]. Nonetheless, such immobilization processes are generally tedious, and the obtained immobilized metal complexes catalysts may still show poor stability.

Recently it is reported that the metal complex could act as a co-monomer that incorporates into the polymer backbone to prepare heterogeneous photocatalysts with remarkable reusability without sacrificing the catalytic activity [22,23]. We expect such polymerization approaches [22,23] may serve as an alternative to conventional

* Corresponding author.
** Corresponding author at: Department of Chemical Engineering, National Taiwan University, Taipei 10617, Taiwan.
E-mail addresses: HIGUCHI.Masayoshi@nims.go.jp (M. Higuchi), wenyueh@ntu.edu.tw (W.-Y. Yu).

https://doi.org/10.1016/j.apcatb.2022.121383
Received 20 January 2022; Received in revised form 3 April 2022; Accepted 5 April 2022
Available online 8 April 2022

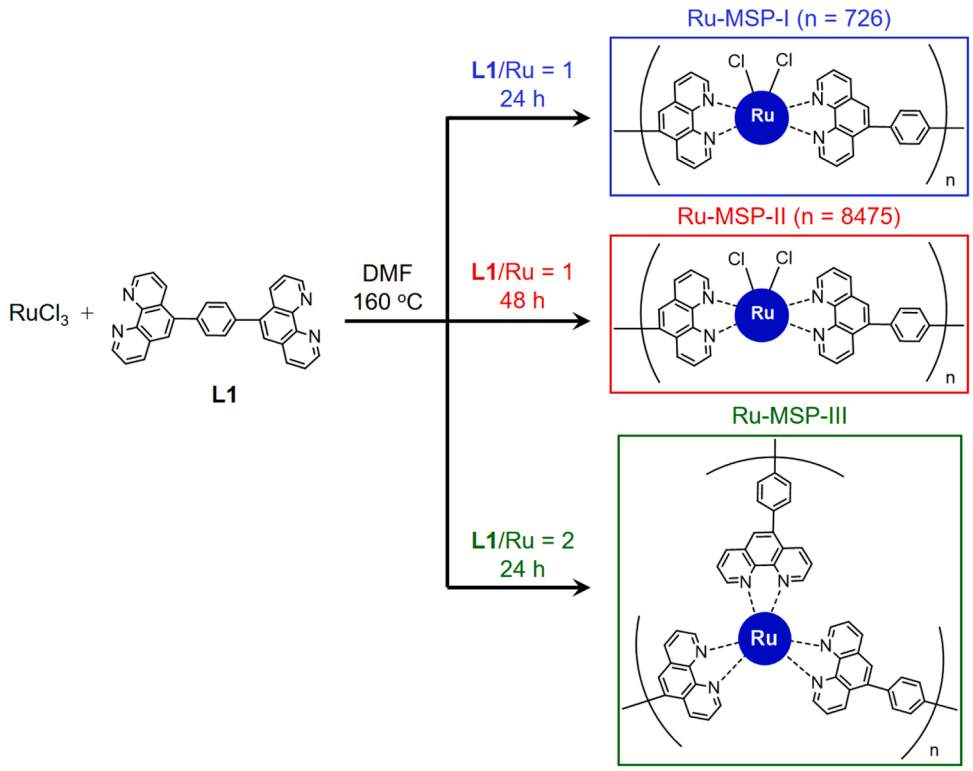

Scheme 1. Synthesis of Ru-MSP catalysts under varied synthesis conditions.

immobilization methods to prepare heterogenized homogeneous metal complex catalysts for CTH reactions. As a subdivision of coordination polymers, metallo-supramolecular polymers (MSPs) are comprised of metal ions and multi-topic organic ligands complexed by coordinating bonding [24]. As a result of the significant electronic interactions between the organic ligands and metal ions, MSPs have been shown to display many unique electrochemical, optical, and magnetic properties, which find versatile applications ranging from energy storage/conversion to electrochromic materials [24–26].

In this work, ruthenium-based metallo-supramolecular polymers (Ru-MSPs) were rationally synthesized by complexing Ru ions with 1,4-bis(1,10-phenanthrolin-5-yl)benzene in an attempt to prepare heterogeneous catalysts for the CTH reaction of carbonyl compounds with formate. It is shown that the degree of polymerization and the local environment of Ru atoms of Ru-MSPs could be controlled by tuning the ligand/metal ratio and the synthesis temperature/period. Combined kinetic data and spectroscopy characterizations reveal that the coordinatively-unsaturated Ru atoms in Ru-MSP are the active sites for the transfer hydrogenation of benzaldehyde to yield benzyl alcohol. The prepared Ru-MSP catalysts are found to be much more active than Ru/C, $RuCl_3$, $Ru(DMSO)_4Cl_2$, and its monomeric analogue, $Ru(phen)_2Cl_2$. According to the density functional theory (DFT) calculations, the improved performance induced by polymerization is attributed to the favorable dehydrogenation of formate and activation of carbonyl oxygen of carbonyl compounds. It is also demonstrated that Ru-MSP catalysts exhibit promising reusability and capability for catalyzing a wide scope of carbonyl compounds under ambient conditions.

2. Experimental section

The manufacturer and purity for chemicals used in this study are summarized in Table S1.

2.1. Synthesis of Ru-MSP Catalysts

A series of Ru-based metallo-supramolecular polymer (Ru-MSP) catalysts were synthesized by complexing Ru ions (from $RuCl_3$) with 1,4-bis(1,10-phenanthrolin-5-yl)benzene (or ligand **L1**) as illustrated in Scheme 1. The ligand **L1** was synthesized by the Suzuki-type cross-coupling reaction of 5-bromo-1,10-phenanthroline with 1,4-benzenediboronic acid bis(pinacol) ester (Scheme S1) as reported in our previous study [27]. The structure of ligand **L1** was verified by the ^{1}H NMR spectrum (Fig. S1).

Ru-MSP catalysts were synthesized by modifying the reported method [28,29] while using **L1** as ligands instead of 1,10-phenanthroline. To synthesize Ru-MSP catalysts with desired physicochemical and catalytic properties, the preparation conditions including the molar ratio of **L1** ligand to Ru ion (**L1**/Ru), synthesis temperature, and synthesis period were systematically investigated in this study. Taking the Ru-MSP-II catalyst as an example, the synthesis procedure is as follows: $RuCl_3$ (Sigma-Aldrich, 1 mmol), **L1** (1 mmol), and LiCl (Sigma-Aldrich, 15 mg) were mixed in dimethylformamide (DMF, Sigma-Aldrich, 20 mL). The obtained solution was degassed and then stirred at 160 °C under nitrogen for 48 h. After that, the mixture was added into acetone (250 mL) and kept at 0 °C overnight for precipitation. The dark purple precipitate was collected by filtration and washed with acetone and water several times, and then dried at 60 °C under vacuum overnight to yield Ru-MSP (90% yield on mass basis).

2.2. Material characterizations

The ultraviolet-visible (UV–VIS) spectra of Ru-MSP catalysts were recorded on a Cary 300nc UV-Visible spectrophotometer. The samples were prepared by dissolving Ru-MSP catalysts in DMSO at room temperature (*ca.* 3×10^{-5} g mL^{-1}). The Fourier-transform infrared (FT-IR) spectra of Ru-MSP catalysts were recorded on a Shimadzu FTIR-8400S spectrometer in transmittance mode with a deuterated triglycine sulfate (DTGS) detector. All FT-IR spectra were averaged from 64 scans

with a resolution of 4 cm^{-1}. ^1H NMR spectra were measured on JEOL AL 300/BZ instrument at 300 MHz. The samples for ^1H NMR were dissolved in deuterated chloroform, and the measured chemical shifts were calibrated using tetramethylsilane (TMS) as the reference. The Ru content of Ru-MSP catalyst was determined by inductively coupled plasma optical emission spectrometry (ICP-OES) on Agilent 720-ES spectrometer. The samples for ICP-OES analysis were prepared by a fusion method with Na_2CO_3 and Na_2O_2. The weight-average molecular weight (MW) of Ru-MSP catalysts were measured using a size exclusion chromatography-viscometry-right angle laser light scattering (SEC-viscometry-RALLS) system [30].

The electronic structure of samples was examined by X-ray absorption spectroscopy (XAS) conducted at beamlines 16 A and 44 A at the National Synchrotron Radiation Research Center (NSRRC), Taiwan. The Ru K-edge X-ray absorption near edge structure (XANES) spectra were recorded at beamline 44 A with a Si(111) monochromator operating at 3 GeV at the Taiwan Photon Source (TPS) with resolving power of 7000 eV and energy resolution of 1.2 eV. Ru foil was used to calibrate the collected Ru K-edge XANES spectra. Cl K-edge XANES spectra were collected at beamline 16 A with a double crystal monochromator (DCM) using the total fluorescence yield (TFY) mode. The electron storage ring was operated at 1.5 GeV with a current of 360 mA, and the resolving power and energy resolution are 5000 and 0.1 eV, respectively. The morphology of samples was observed using field emission transmission electron microscopy (FE-TEM, JEOL JEM-2100 F), and the associated elemental mapping images were recorded with energy-dispersive X-ray spectroscopy (EDS, OXFORD X-MaxN TSR).

2.3. Catalytic testing

The catalytic activity of Ru-MSPs was assessed by the transfer hydrogenation of a variety of carbonyl compounds (aldehydes and ketones) to their corresponding alcohols. Potassium formate was utilized as the hydrogen donor in this study under the reaction conditions similar to literatures [11,31–33]. For each testing, 2 mmol of the carbonyl compound, 6 mmol of HCOOK (0.5 g), and 20 mg of Ru-MSP catalyst (0.033 mmol of Ru) were thoroughly mixed with 1 mL of water and 5 mL of 2-propanol in a 10 mL round-bottom flask equipped with a reflux condenser. Water and 2-propanol are not only used as solvents (to dissolve the potassium formate and to increase the miscibility with benzaldehyde, respectively), but also may both serve as hydrogen donors [4] (Tables S2 and S3). The mixture was stirred at 82 °C using an oil bath for 1 h. After the reaction, the round-bottom flask was removed from the oil bath and cooled by an ice bath. The catalyst was separated from the reaction mixture by vacuum filtration and then washed with ether and water. The unreacted benzaldehyde and produced benzyl alcohol were analyzed quantitatively by a gas chromatograph with a flame ion detector (Agilent 6890 N GC-FID) using dodecane as the internal standard (Fig. S2). Other substrates (*i.e.*, furfural, *p*-tolualdehyde, 2-methoxybenzaldehyde, cuminaldehyde, acetophenone, 2′-methyl--acetophenone, and benzophenone), and their corresponding products were analyzed by ^1H NMR in the $CDCl_3$ solvent after purification. For ^1H NMR analyses, the DMSO solvent (0.7 mmol) was added as the internal standard.

2.4. Density functional theory (DFT) calculations

The octahedral coordination geometry was selected to model the Ru $(phen)_2Cl_2$ complex (the monomeric analogue of Ru-MSP), the Ru-MSP trimer, and the Ru-MSP pentamer. Geometry optimization and single-point energy calculations were performed using DFT at the B3LYP [34,35] /def2-SVP [36] and B3LYP/def2-TZVP levels of theory, respectively. Frequency calculations were carried out on all structures to ensure convergence to true local minimum. The *cis* position of the 1, 10-phenanthroline ligands was selected for demonstration because of the lower electronic energy compared to the *trans* configuration. All DFT calculations were performed using a development version of the Q-Chem software package [37]. The partial charges on atoms were calculated using the NBO 7.0 program [38].

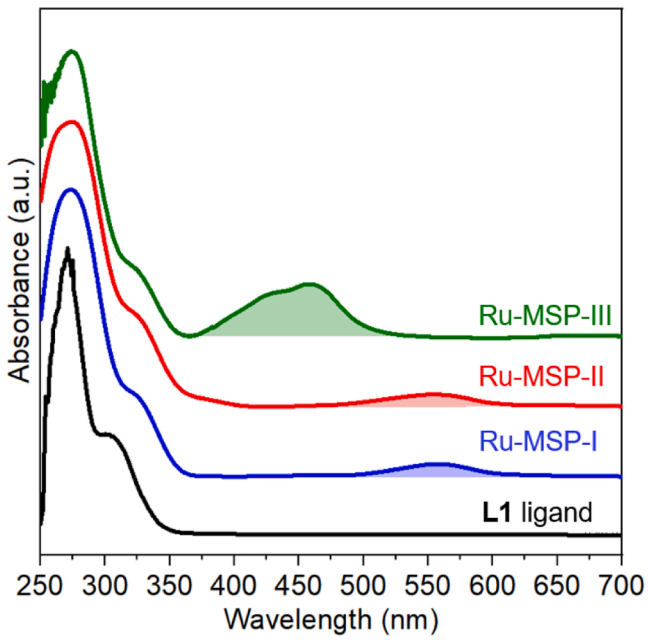

Fig. 1. UV–vis spectra of **L1** ligand and Ru-MSP catalysts.

3. Results and discussion

3.1. Syntheses and characterizations of Ru-MSP catalysts

As mentioned in the Experimental section, we have attempted to optimize Ru-MSP catalysts in this study by changing the preparation conditions including the molar ratio of **L1** ligand to Ru ion (**L1**/Ru ratio), synthesis temperature, and synthesis period. It is found that no precipitate was obtained after the work-up procedure when the **L1**/Ru ratio, synthesis temperature, and synthesis period were set at unity, 140 °C, and 24 h, respectively. We interpret this result as the temperature at 140 °C is not high enough to provide sufficient energy to facilitate the complexation between the Ru ions and **L1** ligands. When the synthesis temperature was increased from 140° to 160°C, a solid catalyst was obtained (designated as Ru-MSP-I, Scheme 1). The weight-average molecular weight of Ru-MSP-I determined by SEC-viscometry-RALLS system is 4.4×10^5 Da, which corresponds to a degree of polymerization (DP; the number of monomeric units in polymer) of *ca.* 726. The polymerized structure of Ru-MSP-I will be discussed later in detail based on XAS characterizations. As noted in the later section, the Ru-MSP-I catalyst suffers a significant mass loss during the catalytic reaction, signifying its dissolution in the reaction medium, which is presumably due to its low degree of polymerization.

To address the stability issue of Ru-MSP-I, two synthesis approaches were then adopted in this work, *i.e.*, (1) extending the synthesis period from 24 to 48 h, and (2) increasing the **L1**/Ru ratio from unity to two, in an attempt to increase the weight-average molecular weight of Ru-MSP catalysts. The solid catalyst obtained with a synthesis period of 48 h was designated as Ru-MSP-II (Scheme 1), and its weight-average molecular weight is 5.3×10^6 Da (the corresponding DP is *ca.* 8745), which is approximately an order of magnitude higher than that of Ru-MSP-I. As discussed in the later section, the Ru-MSP-II catalyst is very stable and active during the catalytic reaction. The solid catalyst obtained with a **L1**/Ru ratio of two was designated as Ru-MSP-III (Scheme 1). Unfortunately, the weight-average molecular weight of Ru-MSP-III is unable to be determined in this study as it does not fully dissolve in the DMSO

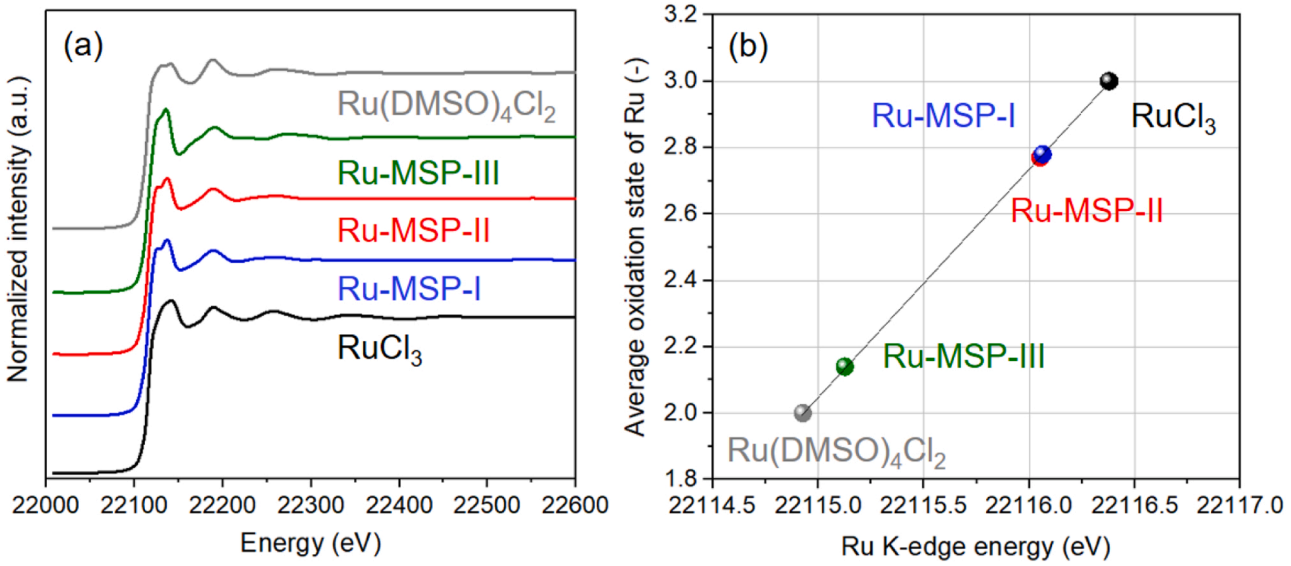

Fig. 2. (a) Ru K-edge XANES spectra, and (b) oxidation state of Ru atom of Ru-MSP catalysts, $RuCl_3$, and $Ru(DMSO)_4Cl_2$.

solvent for the SEC-viscometry-RALLS analysis. Nonetheless, it is found that Ru-MSP-III does not dissolve in the reaction medium, which is suggestive of a high degree of polymerization.

UV–VIS spectroscopy is employed to investigate the complexation between **L1** ligands and Ru ions in the prepared Ru-MSP catalysts. As shown in Fig. 1, the **L1** ligand shows an absorbance speak at a wavelength of *ca.* 267 nm with a shoulder at *ca.* 300 nm in the UV light region of its UV–VIS spectrum, which is attributed to the π-π * transition of its phenanthroline units [27]. As compared to the **L1** ligand, such peak and shoulder for all of the Ru-MSP catalysts are blue-shifted to *ca.* 273 and 330 nm, respectively, due to the complexation between **L1** ligand and Ru ions [27]. In contrast to the **L1** ligand, another distinct feature is that all of the Ru-MSP catalysts display a visible-light absorption band in their UV–VIS spectra, which is due to the metal to ligand charge transfer (MLCT) [39] from the d-orbital of Ru to the π * -orbital of **L1** ligand. According to literatures [40–42], the presence of MLCT absorbance band suggests the presence of Ru^{2+} ions in Ru-MSP catalysts (it is noted that there is no such absorbance for Ru^{3+} ions). The average oxidation state of Ru atom in Ru-MSP catalysts will be further discussed using XANES characterizations. For Ru-MSP-I and Ru-MSP-II, the positions of absorbance band due to MLCT are quite similar (at between 470 and 630 nm), suggestive of a similar local structure formed by Ru ions and **L1** ligands in Ru-MSP-I and Ru-MSP-II. By contrast, the MLCT absorbance band of Ru-MSP-III is in the range from 360 to 560 nm, signifying that Ru-MSP-III possesses a structure different from those of Ru-MSP-I and Ru-MSP-II. The MLCT band of Ru-MSP-III is similar to that of dichlorotris(1, 10-phenanthroline)-ruthenium(II) complex reported in literature [43]. It is noted that although the structural differences between Ru-MSP catalysts are not discernible in their infrared spectra (Fig. S3), they are easily distinguishable in their EXAFS spectra as discussed in the later section.

X-ray absorption spectroscopy (XAS) was used to characterize the electronic structure of Ru-MSP catalysts prepared in this study. Fig. 2a depicts the Ru K-edge XANES spectra of Ru-MSP catalysts and reference compounds including $RuCl_3$ and $Ru(DMSO)_4Cl_2$. It is well-known that the absorption edge energy of an atom is related to its oxidation state; in general, the absorption edge of an atom is shifted to a higher energy when its oxidation state is increased [44–46]. Accordingly, by comparing the absorption edges of an atom with those of known oxidation states, one could determine the average oxidation state of atom in the compounds investigated [47]. The edge energies of Ru K-edge XANES spectra for $RuCl_3$ (oxidation state for Ru is 3 +) and Ru

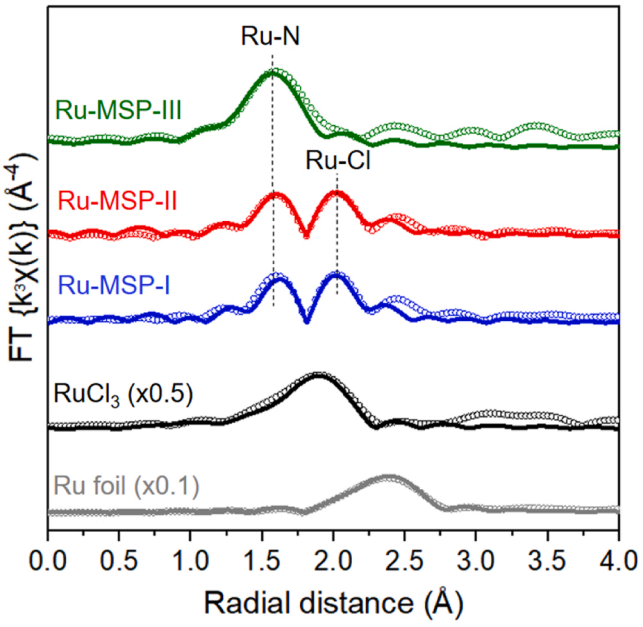

Fig. 3. R-space spectra of Ru K-edge EXAFS of Ru-MSP catalysts, $RuCl_3$, and Ru foil. The fitting of data points (shown as circles) is presented as the solid line.

$(DMSO)_4Cl_2$ (oxidation state for Ru is 2 +) are 2,2116.4 and 2, 2114.9 eV, respectively. According to the measured edge energies, the average oxidation states of Ru atom in Ru-MSP-I, Ru-MSP-II, and Ru-MSP-III were determined to be 2.78, 2.77, and 2.14, respectively (Fig. 2b). These results also suggest that the local structures of Ru atoms in Ru-MSP-I and Ru-MSP-II are similar but differ from that of Ru-MSP-III, which is consistent with the observations in their UV–VIS spectra (Fig. 1).

The local structure surrounding the Ru atom in Ru-MSP catalysts is investigated by analyzing their EXAFS spectra. Fig. S4 and Fig. 3 depict the K-space and R-space data of EXAFS spectra, respectively, and the associated fitting results are summarized in Table 1. For comparison, the EXAFS spectra of Ru foil and $RuCl_3$ are included. As shown in Fig. 3, all Ru-MSP catalysts display a peak with a radial distance of *ca.* 1.6 Å, which has been attributed to the Ru-N bonding in the previous studies [44,48,49]. The presence of Ru-N bonding in all Ru-MSP catalysts is

Table 1
The local structure parameters of Ru-MSP catalysts estimated by EXAFS analysis.

Sample	Shell	C. N.[a]	R (Å)[b]	$\sigma^2 \times 10^{-3}$ (Å^2)[c]	R-factor	Reduced χ-square
Ru-MSP-I	Ru-N	4	2.13(1)	2.3(9)	0.031	5512
	Ru-Cl	2	2.366 (1)	2.2(9)		
Ru-MSP-II	Ru-N	4	2.12(1)	2.5(9)	0.019	659
	Ru-Cl	2	2.368 (1)	2.4(7)		
Ru-MSP-III	Ru-N	6	2.07(1)	4.2(8)	0.036	4550
$RuCl_3$	Ru-Cl	6	2.34(2)	7(1)	0.049	8743
Ru foil	Ru-Ru	12	2.681 (5)	4.6(2)	0.004	4542

[d] numbers in parentheses represent the error in the last digit.
[a] coordination number.
[b] interatomic distance.
[c] Debye-Waller factor.

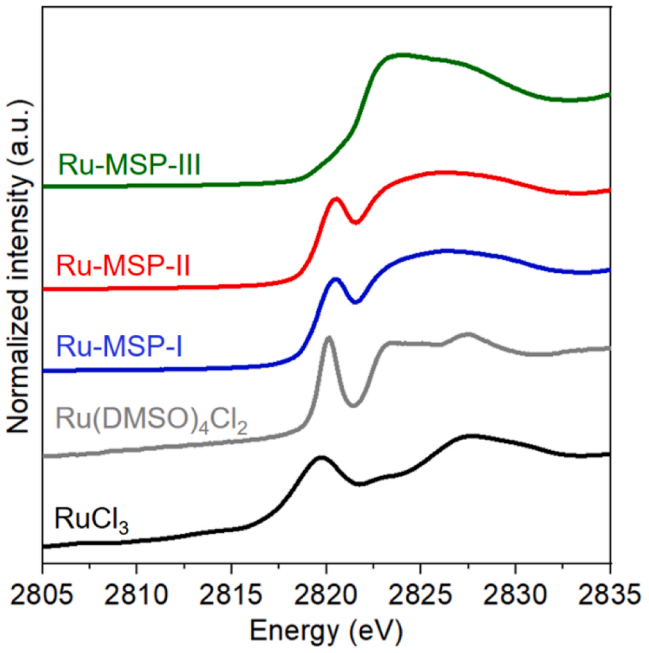

Fig. 4. Cl K-edge XANES spectra of Ru-MSP catalysts, $RuCl_3$, and $Ru(DMSO)_4Cl_2$.

consistent with the fact that the Ru ion complexes with **L1** ligand as observed in their UV–VIS spectra (Fig. 1). Both Ru-MSP-I and Ru-MSP-II exhibit a peak with a radical distance of 2 Å, which is associated with the presence of Ru-Cl bonding [48], where the Cl is believed to originate from the $RuCl_3$ precursor (Scheme 1). As discussed later, the Ru-Cl bonding is readily dissociated during the catalytic reaction. Accordingly, the observed Ru-Cl bonding manifests that the Ru atoms in Ru-MSP-I and Ru-MSP-II are coordinatively-unsaturated, *i.e.*, the Ru atoms are not completely coordinated with the N atoms of **L1** ligand (Scheme 1). As fitted by EXAFS analyses, the Ru atom in Ru-MSP-I and Ru-MSP-II coordinates with four N atoms and two Cl atoms (Table 1). The presence of coordinatively-unsaturated Ru atoms in Ru-MSP catalysts is crucial to their catalytic transfer hydrogenation activity, which will be discussed in the later sections. In contrast to Ru-MSP-I and Ru-MSP-II, Ru-MSP-III does not show a significant peak at *ca.* 2 Å, suggesting that the Ru-Cl bonding is nearly absent in Ru-MSP-III. In other words, the Ru atoms in Ru-MSP-III are coordinatively-saturated, *i.e.*, completely coordinated with the N atoms in **L1** ligand (Scheme 1) without bonding to the Cl atoms. EXAFS analyses show that the Ru atom in Ru-MSP-III coordinates with six N atoms of **L1** ligands (Table 1).

A peak with a radical distance of 2.4 Å is observed for the reference Ru foil due to the Ru-Ru bonding.[50,51] Such peak due to Ru-Ru bonding is relatively insignificant for the synthesized Ru-MSP catalysts, suggesting that Ru atoms are well dispersed in their polymerized structures. In line with EXAFS characterizations, Fig. S5 shows the FE-TEM image and the corresponding elemental mapping of Ru-MSP-II, in which Ru atoms are found to be well dispersed on Ru-MSP-II. It is noted that the Ru loading in Ru-MSP-II determined by ICP-OES is 16.8 wt% (agrees with its theoretical Ru loading of 16.6 wt%). Such high Ru loading does not lead to the aggregation of Ru atoms on Ru-MSP-II, which is believed to benefit from the complexation with **L1** ligand that highly disperses the Ru ions.

The Cl K-edge spectra were measured to provide the complementary information to the coordination environment between Ru atoms and Cl atoms in Ru-MSP catalysts. Fig. 4 depicts the Cl K-edge spectra of Ru-MSP catalysts and reference compounds including $RuCl_3$ and $Ru(DMSO)_4Cl_2$. The pre-edge absorption at *ca.* 2821–2822 eV is attributed to the electronic transition from Cl 1 *s* orbital to Ru 4*d* orbital when the Cl atom is bound to the Ru atom in Ru-containing complexes [52]. It is observed that references $RuCl_3$ and $Ru(DMSO)_4Cl_2$ display the pre-edge absorption peak with energy positions in their Cl K-edge spectra at *ca.* 2819.7 and 2820.1 eV, respectively. The Cl K-edge spectra of Ru-MSP-I and Ru-MSP-II are similar with a pre-edge absorption peak at *ca.* 2820.5 eV. These results confirm the presence of Ru-Cl bonding in Ru-MSP-I and Ru-MSP-II as mentioned above by the characterizations based on Ru K-edge EXAFS (Fig. 3). It is noted that such Ru-Cl bonding is absent in Ru-MSP-III as the pre-edge absorption peak due to the electronic transition from Cl 1 *s* orbital to Ru 4*d* orbital is not observed. These results support that Ru atoms in Ru-MSP-III are coordinately saturated with N atoms (with a coordination number of six), and the Cl ions just serve as counter ions without bonding to the Ru atoms.

3.2. Catalytic performance of Ru-MSP catalysts

The transfer hydrogenation of benzaldehyde (C_6H_5CHO, or PhCHO) with formate ($HCOO^-$) to yield benzyl alcohol ($C_6H_5CH_2OH$, or $PhCH_2OH$) was employed as the model reaction to investigate the carbonyl reduction activity of prepared Ru-MSP catalysts in this study. The results of reaction testing including the conversion of benzaldehyde (X_{PhCHO}) and yield of benzyl alcohol (Y_{PhCH_2OH}) of Ru-based catalysts are summarized in Fig. 5a. Reference catalysts such as Ru/C, $RuCl_3$, and $Ru(DMSO)_4Cl_2$ are also included for comparison. It is noted that some of the Ru-based catalysts tested in this study are regarded as homogeneous catalysts as they are dissolved in the reaction medium (Fig. 5b). As shown in Fig. 5a, both Ru-MSP-I and Ru-MSP-II are highly active to convert benzaldehyde to form benzyl alcohol ($X_{PhCHO} = Y_{PhCH_2OH} =$ 100%), while Ru-MSP-III displays no benzaldehyde conversion under the same reaction condition. The specific surface areas of Ru-MSP-I, Ru-MSP-II, and Ru-MSP-III are 14, 8, and 38 $m^2\ g^{-1}$, respectively (Fig. S6), which is of low relevance with their catalytic activities. As indicated by EXAFS characterizations (Fig. 3), Ru-MSP-I and Ru-MSP-II (prepared with **L1**/Ru ratio = 1) both possess coordinatively-unsaturated Ru sites (*i.e.*, not completely bonded with the N atoms of **L1** ligand), which are absent in Ru-MSP-III (prepared with **L1**/Ru ratio = 2). Based on these observations, it was hypothesized that the lack of coordinatively-unsaturated Ru sites is the main origin of the poor catalytic performance of Ru-MSP-III on the conversion of benzaldehyde to benzyl alcohol. To test this hypothesis, another sample that contain only coordinatively-saturated Ru sites (denoted as $Ru\text{-}MSP_{SAT}$) was prepared (Scheme S2) using 1,4-bis(2,2′:6′,2′-terpyridine-4-yl)benzene (**L2**), a ligand with six coordination sites. It is found that $Ru\text{-}MSP_{SAT}$ does not show any benzaldehyde conversion under the same reaction condition, which supports the above hypothesis that coordinatively-saturated Ru sites are not catalytically active. These results demonstrate that the presence of coordinatively-unsaturated Ru sites is crucial to the transfer

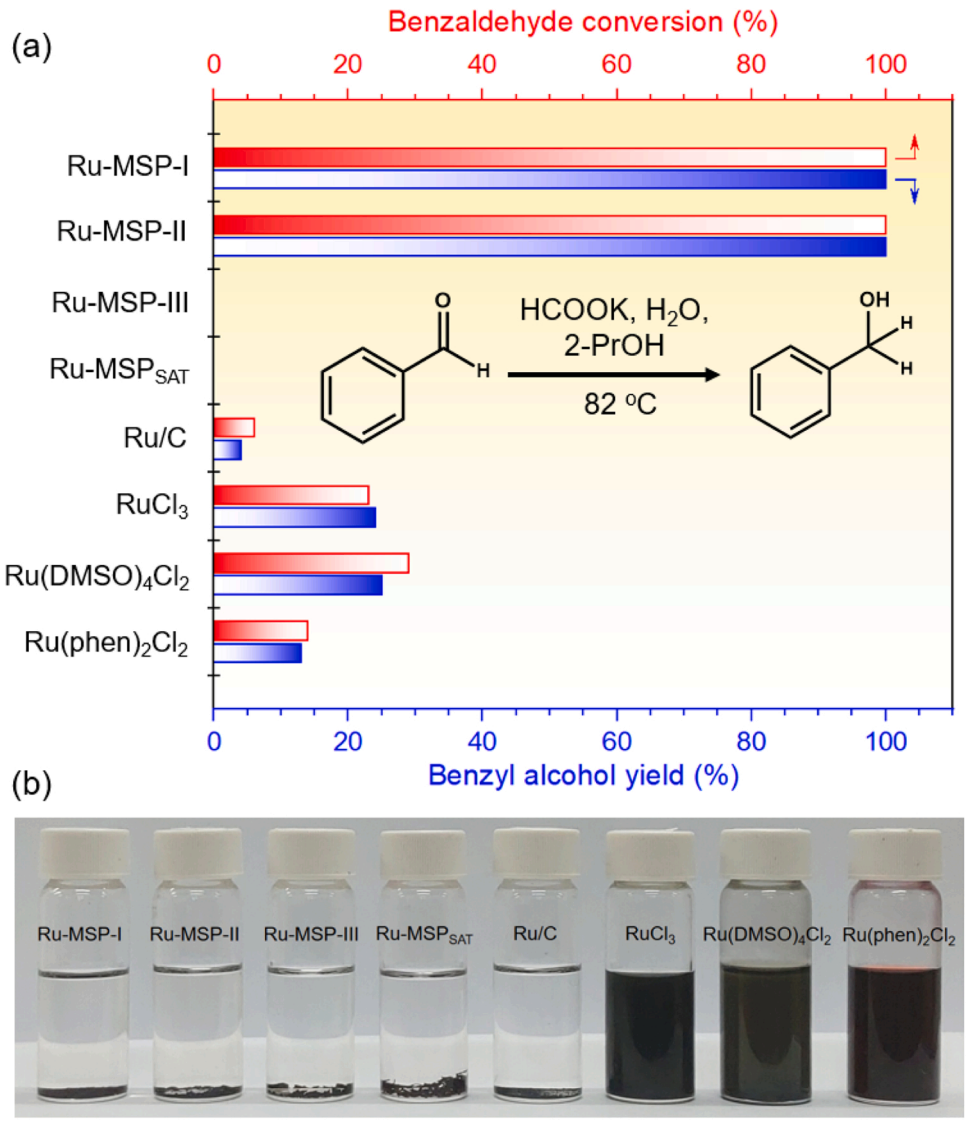

Fig. 5. (a) Activity test results of Ru-MSP and commercial Ru catalysts (benzaldehyde, 2 mmol; HCOOK, 6 mmol; water 1 mL; 2-propanol 5 mL; 82 °C, 1 h; Ru in each testing is 0.033 mmol). (b) Photograph of Ru-based catalysts in the reaction medium.

hydrogenation of benzaldehyde with formate to yield benzyl alcohol. The coordinatively unsaturated site (CUS) has been recently reported as the active center in metal-organic frameworks (MOFs) [53,54], a subcategory of coordination polymers.

It is noted that even though Ru-MSP-I is highly active to hydrogenate benzaldehyde to benzyl alcohol, it suffers a significant mass loss (*ca.* 20%) after the recovery, which is suggestive of its dissolution during the catalytic reaction. In contrast, Ru-MSP-II is found to be very stable during the catalytic reaction as indicated by its high recovery after the reaction testing (> 95%; the slight mass loss may occur during the vacuum filtration to separate the catalyst from the reaction medium). As mentioned above, the weight-average molecular weights of Ru-MSP-I and Ru-MSP-II are 4.4×10^5 and 5.3×10^6 Da, respectively. Apparently, the resistance to dissolution of Ru-MSP catalysts during the catalytic reaction can be enhanced by increasing their molecular weight, which was achieved by prolonging the synthesis period from 24 to 48 h. ^{1}H NMR analysis was employed to examine the possible presence of by-products from the benzaldehyde conversion over Ru-MSP-II. As shown in Fig. S7, no by-products such as toluene and cyclohexanecarboxaldehyde were found, indicative of a 100% selectivity from benzaldehyde to form benzyl alcohol over Ru-MSP-II.

The commercially-available Ru-based materials including Ru/C, $RuCl_3$, and $Ru(DMSO)_4Cl_2$ were also tested for their performance on the catalytic transfer hydrogenation of benzaldehyde under the same reaction condition (Fig. 5a), in which both $RuCl_3$ and $Ru(DMSO)_4Cl_2$ are regarded as homogeneous catalysts due to their high solubility in the reaction medium (Fig. 5b). It is shown that among them the most active is $Ru(DMSO)_4Cl_2$ (X_{PhCHO} = 29%), followed by $RuCl_3$ (X_{PhCHO} = 24%), and the least active is Ru/C (X_{PhCHO} = 6%). Despite their higher activities than Ru/C, $Ru(DMSO)_4Cl_2$ and $RuCl_3$ are not desired as they are difficult to be recovered for the next catalytic use. As shown in Fig. 5a, all of these commercially-available Ru-based materials are much less active than Ru-MSP-II in the transfer hydrogenation of benzaldehyde to form benzyl alcohol on the basis of the same amount of Ru content, indicating that Ru-MSP-II represents a promising heterogeneous catalyst capable of the catalytic reduction of carbonyl compounds. The plausible mechanism for the transfer hydrogenation of benzaldehyde to benzyl alcohol catalyzed by Ru-MSP-II will be discussed in the later section.

In order to further explore the effect of polymerization on the transfer hydrogenation activity, the monomeric analogue of Ru-MSP-II, *i.e.*, the $Ru(phen)_2Cl_2$ complex, was synthesized using 1,10-phenantroline as the ligand (Scheme S3) and tested under the same reaction condition (Fig. 5a). It is found that the conversion of benzaldehyde over $Ru(phen)_2Cl_2$ is only *ca.* 14%, indicating that Ru-MSP-II is much more

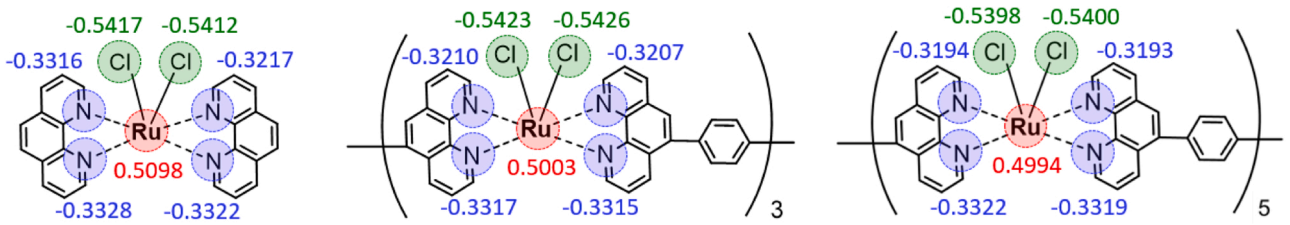

Fig. 6. Calculated charge distribution of $Ru(phen)_2Cl_2$, Ru-MSP trimer and Ru-MSP pentamer.

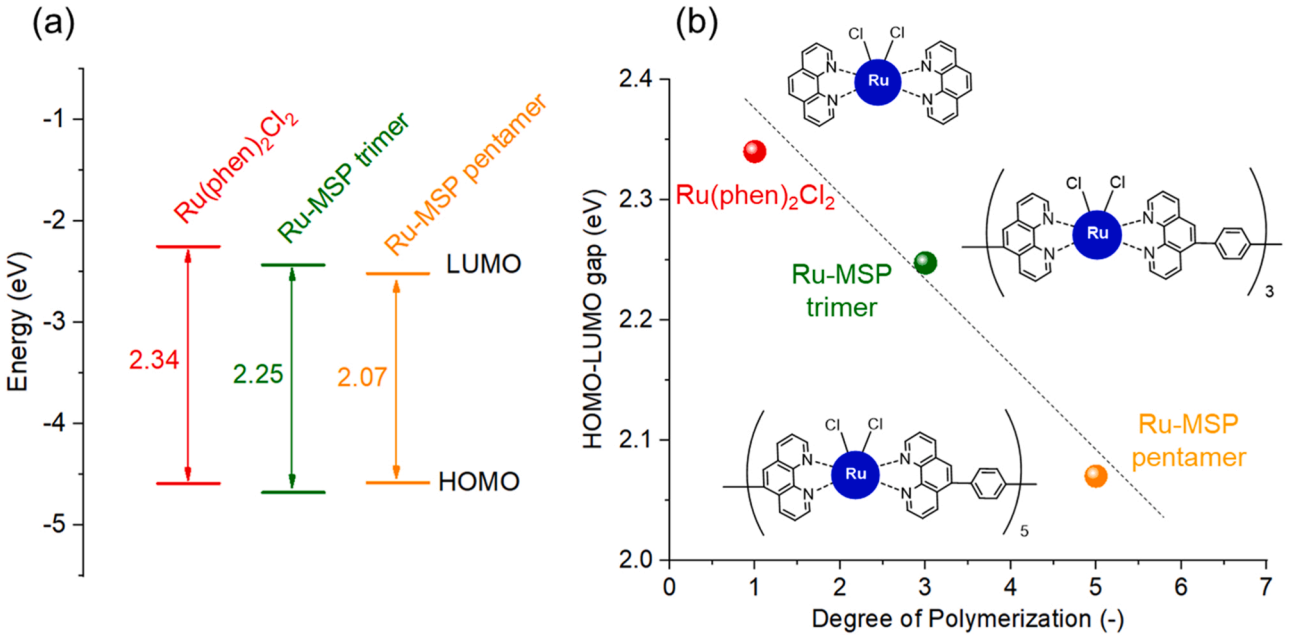

Fig. 7. (a) Calculated HOMO-LUMO energy level, and (b) HOMO-LUMO gap of $Ru(phen)_2Cl_2$, Ru-MSP trimer and Ru-MSP pentamer.

active than its monomeric analogue. In other words, the formation of polymerized structure not only heterogenize the homogeneous Ru pincer complexes but also results in an enhanced activity on the transfer hydrogenation of carbonyl compounds.

3.3. *Plausible reaction mechanism*

The reaction mechanism and the origin of the polymerization-induced activity enhancement for the transfer hydrogenation of benzaldehyde to benzyl alcohol with formate over the Ru-MSP catalyst were discussed in terms of the calculated charge distributions (Fig. 6) and energy levels (Fig. 7) of $Ru(phen)_2Cl_2$, Ru-MSP trimer, and Ru-MSP pentamer. It is noted that the oligomers of Ru-MSP were used to simplify the calculation work.

Fig. 6 shows the calculated charge distributions of $Ru(phen)_2Cl_2$ and Ru-MSP oligomers. In all cases, the centered Ru atom carries a partial positive charge and the surrounding atoms in **L1** ligand including N and Cl atoms have partial negative charges. It is found that when the degree of polymerization is increased, the partial charge on the Ru atom is gradually decreased, which is consistent with the XANES observations (Fig. 2b), where the Ru atom in Ru-MSP with higher degree of polymerization is of a lower average oxidation state. The decrease in positive charge reflects that the electron density of the Ru atom increases with increasing degree of polymerization.

It is noted that the electron enrichment on metal nanoparticles has been proposed [13, 55–57] as a key property to enable the bridged adsorption of formate through the strong back donation, thus facilitating the selective cleavage of the C-H bond, the rate-determining step for dehydrogenation of fomate [6,13,57]. Taking Pd nanoparticles as an example, the electron enrichment mentioned above could be realized by (1) adding a second metal (*e.g.*, Ag) to prepare bimetallic nanoparticles with a shell-core structure, where the second metal in the core region has a large difference in the work function in relation to Pd, thus providing strong electron promotion to Pd shell [58], or by (2) immobilizing Pd nanoparticles onto a semiconductor support (*e.g.*, graphitic carbon nitride) forming an interfacial Mott-Schottky heterojunction that enables electron transfer from the support to the supported Pd nanoparticles [10]. In the present work, the electron transfer from the **L1** pincer ligand to the centered Ru atom is found to be enhanced by increasing the degree of polymerization. Accordingly, the higher benzyl alcohol yield observed on polymerized Ru-MSP-II as compared to its monomeric analogue, $Ru(phen)_2Cl_2$, (Fig. 5a) could be attributed to the higher catalytic activity toward formate dehydrogenation due to polymerization-induced electron enrichment on Ru atoms.

The calculated energy levels of $Ru(phen)_2Cl_2$, Ru-MSP trimer, and Ru-MSP pentamer are shown in Fig. 7a. The energy levels of the highest occupied molecular orbital (HOMO) of $Ru(phen)_2Cl_2$, Ru-MSP trimer, and Ru-MSP pentamer are similar, suggesting that the d-orbitals of Ru atoms in these compounds have similar energy levels. It is found that as the degree of polymerization is increased, the energy level of the lowest unoccupied molecular orbital (LUMO) gradually decreases from −2.25 to −2.52 eV. The reduction of LUMO energy level suggests that the energy level of π * -orbital of ligand decreases with increasing degree of polymerization. When the degree of polymerization increases, the energy gap between HOMO and LUMO decreases (Fig. 7b), which are conceptually consistent with the trend suggested by UV–VIS spectra of

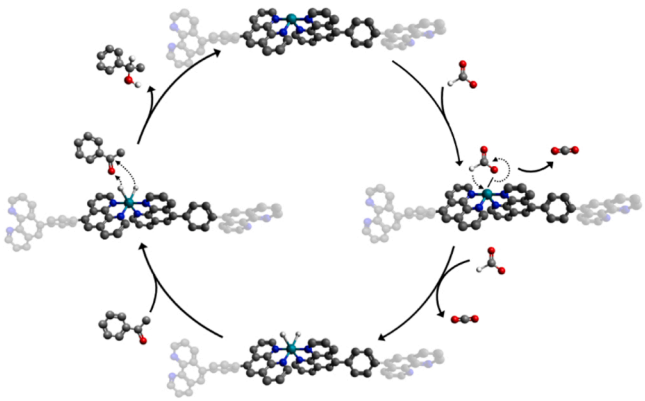

Scheme 2. Proposed mechanism for transfer hydrogenation of benzaldehyde with formate over Ru-MSP catalyst (white: H atom; gray: C atom; red: O atom; blue: N atom; cyan: Ru atom).

$Ru(phen)_2Cl_2$ and Ru-MSP-II (Fig. S8).

It is noted that the lower LUMO energy level could indicate a higher electrophilicity, *i.e.*, a higher Lewis acidity that is available to interact with Lewis bases [59,60]. Therefore, the reducing LUMO energy level of ligand moieties suggests that the ligand electrophilicity is enhanced with the increasing degree of polymerization. In the Lewis acid-assisted carbonyl reduction, the interactions with carbonyl oxygen in either substrate or key intermediate play an important role as they could govern the associated reaction thermodynamics and kinetics by activating the substrate, and/or stabilizing the intermediate [61]. We expect that the surface sites of catalyst with an enhanced electrophilicity could exhibit a higher tendency to interact with the lone pair of carbonyl oxygen, thus facilitating the adsorption of carbonyl group for subsequent reduction with surface hydrogen. Therefore, the fact that the polymerized Ru-MSP-II exhibits a higher benzyl alcohol yield than its monomeric analogue, $Ru(phen)_2Cl_2$, (Fig. 5a) is likely due to the enhanced ligand electrophilicity induced by polymerization, by which promotes the activation of carbonyl group in benzaldehyde.

Based on above discussions, a plausible reaction mechanism of the transfer hydrogenation of benzaldehyde with formate over the Ru-MSP catalyst to benzyl alcohol is proposed as illustrated in Scheme 2. The formates dehydrogenate on the coordinatively-unsaturated Ru site in Ru-MSP to form adsorbed hydrogen atoms, which are available for the subsequent transfer hydrogenation to benzaldehyde. It is believed that the electron transfer from the surrounding pincer ligands to the centered Ru atom (or electron enrichment) is beneficial to selectively dissociate the C-H bonding in formate to form adsorbed hydrogen atom (with CO_2 as the by-product), thus promoting the following transfer hydrogenation process. The benzaldehyde is activated at the phenanthroline moiety in Ru-MSP with its carbonyl oxygen through the Lewis acid-base interactions. In the activation of benzaldehyde, the ligand electrophilicity (or Lewis acidity) plays an important role by interacting with the lone pair of carbonyl oxygen (Lewis base) in benzaldehyde. The activated benzaldehyde is further reduced by the adsorbed hydrogen atoms on the coordinatively-unsaturated Ru site to form benzyl alcohol. Our theoretical calculations reveal that the electron transfer from ligands to Ru atoms and the ligand electrophilicity could be both enhanced by polymerization, thus explaining the higher catalytic activity of polymerized Ru-MSP catalyst as compared to its monomeric analogue. It is noted that some literatures [62–64] have proposed a plausible mechanism involving the nucleophilic addition of water to the adsorbed formate to form an intermediate for producing dihydrogen from the aqueous formate solution. In order to investigate the possibility of water as the hydrogen source, a control experiment was carried out using D_2O instead of H_2O in the reaction medium (Table S3). It is found that the benzaldehyde conversion is lower (55%) while the proportion of deuterated benzyl alcohol is not increased when D_2O was employed. These observations suggest the participation of water in catalysis but do not support the hydrogen transfer from water into benzyl alcohol. Further mechanistic investigations are undertaken in an attempt to explore the participation role of water in the catalytic transfer hydrogenation with formate.

3.4. Stability, reusability, and substrate scope of Ru-MSP catalysts

Apart from the catalytic performance (*e.g.*, reactant conversion and product selectivity), the stability, reusability, and substrate scope are also crucial for practical applications of heterogeneous catalysts. To examine the heterogeneity of Ru-MSP-II, two parallel reaction tests, *i.e.*, the transfer hydrogenation of benzaldehyde to benzyl alcohol with and without hot filtration, were conducted as shown in Fig. 8a. It is shown

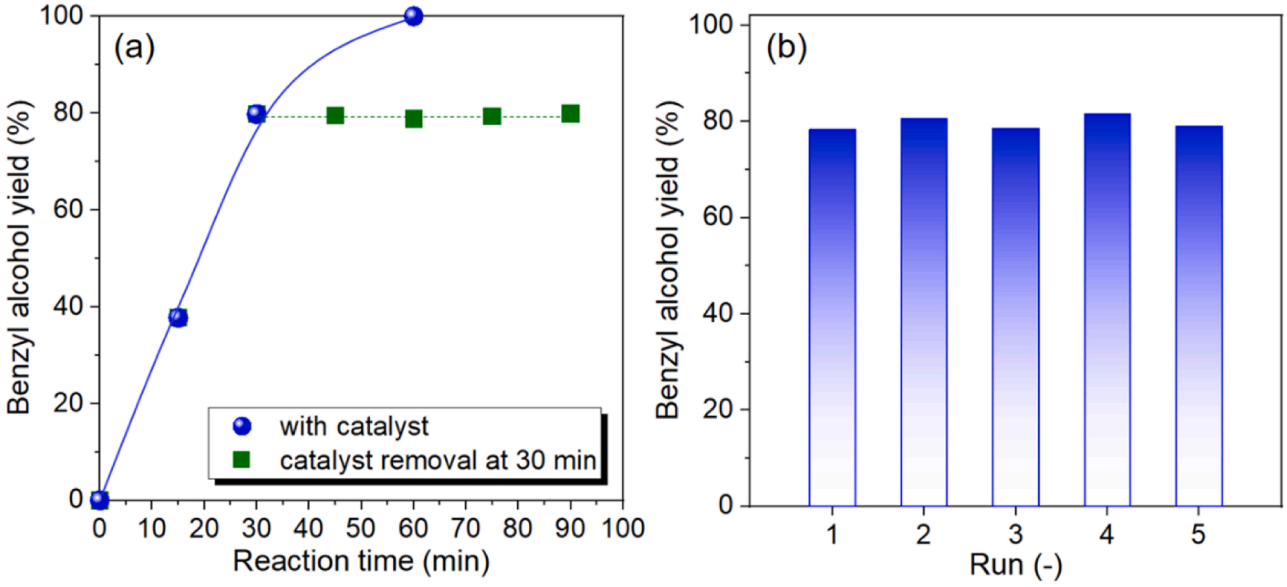

Fig. 8. (a) Hot filtration test of Ru-MSP-II: filtered out the solid catalyst after 30 min and then the reaction was continued without the solid catalyst (reaction conditions: benzaldehyde, 2 mmol; HCOOK, 6 mmol; water, 1 mL; 2-propanol, 5 mL; Ru-MSP-II, 20 mg; 82 °C, 1 h). (b) reuse test of Ru-MSP catalyst in CTH of benzaldehyde. (reaction conditions: benzaldehyde, 2 mmol; HCOOK, 6 mmol; water, 1 mL; 2-propanol, 5 mL; Ru-MSP-II, 10 mg; 82 °C, 1 h).

Table 2
Catalytic transfer hydrogenation of a variety of carbonyl compounds over Ru-MSP-II.[a].

Entry	Reactant	Product	Time (h)	Conversion (%)	Selectivity (%)[b]
Aldehydes					
1			1	100	100
2	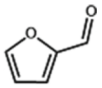	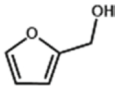	1	100	100
3	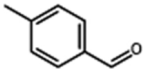	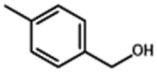	2	100	100
4	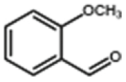	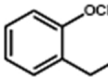	2	100	100
5	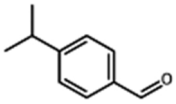	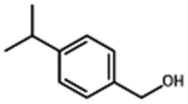	3	100	100
Ketones					
6	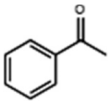	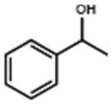	2	67	100
7	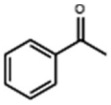	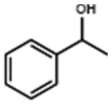	3	> 99	100
8	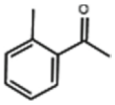	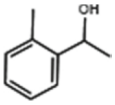	3	44	100
9	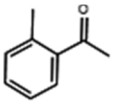	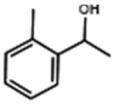	6	97	100
10	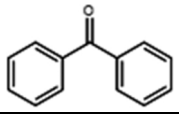	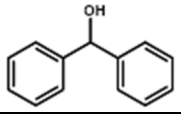	6	100	100

[a] reaction condition: substrate, 2 mmol; HCOOK, 6 mmol; water 1 mL; 2-propanol 5 mL; Ru-MSP-II, 20 mg; reaction temperature = 82 °C.
[b] the possible products are described in supporting materials with the ^{1}H NMR spectrum of reaction mixture.

that as the reaction time was gradually increased, the yield of benzyl alcohol in the presence of Ru-MSP-II first increased to 40% at 15 min, then to 80% at 30 min, and finally reached 100% at 1 h. In the separate reaction test, no increase in the yield of benzyl alcohol was observed after Ru-MSP-II was removed by hot filtration at 30 min. Furthermore, no Ru species was detected in the aliquots of the reaction mixture by ICP-OES. These results clearly indicate that no active component was leached from Ru-MSP-II into the reaction medium, thus demonstrating the heterogeneity and stability of Ru-MSP-II.

The used Ru-MSP-II was recovered after the catalytic reaction by vacuum filtration to further investigate the reusability. The recovered Ru-MSP-II was washed with DI water and acetone, followed by drying in vacuum overnight. Such reaction testing and recovery were repeated for five times, and the catalytic performance was expressed as the yield of benzyl alcohol as shown in Fig. 8b. It is shown that the Ru-MSP-II is highly reusable as it displays *ca.* 80% yield of benzyl alcohol without any observed activity decay in the continuous five catalytic cycles. It is noted that the fresh and used Ru-MSP-II show no insignificant differences in their UV–VIS spectra (Fig. S9), IR spectra (Fig. S10), and FE-TEM images (Figs. S5 and S11), which are in line with the fact that Ru-MSP-II is highly stable under reaction conditions. Fig. S12 depicts the R-space spectra of Ru K-edge EXAFS of fresh and used Ru-MSP-II, where it is found that the Ru-N bonding retains while Ru-Cl bonding disappears after the catalytic reaction. The disappearance of Ru-Cl bonding in Ru K-edge EXAFS spectra supports that the Ru-Cl bond in Ru-MSP-II readily dissociates under reaction conditions, thus resulting in the coordinatively-unsaturated Ru sites for the dehydrogenation of formate as suggested in Scheme 2.

A variety of carbonyl compounds were examined to investigate the scope of substrates for the catalytic transfer hydrogenation with formate over Ru-MSP-II as listed in Table 2. The carbonyl compounds tested in this study include the benzylic carbonyls (*i.e.*, benzaldehyde, and acetophenone), their substituted counterparts (*i.e.*, *p*-tolualdehyde, 2-methoxybenzaldehyde, cuminaldehyde, 2′-methyl-acetophenone, and benzophenone), and the furfural, a renewable platform compound derived from lignocellulosic biomass [65].

Reaction testing results (Table 2) reveal that all of these carbonyl compounds examined can be efficiently converted into their corresponding alcohols over Ru-MSP-II through the catalytic transfer hydrogenation with formate. Similar results were observed between the benzaldehyde and its ketone counterpart, *i.e.*, acetophenone. Even though the time to achieve 100% conversion is prolonged when the substituents (*e.g.*, methyl, methoxy, *etc.*) are present on the benzene ring of benzylic carbonyls, the selectivity to the corresponding alcohols is

unchanged at 100% (the ^{1}H NMR spectra are provided in Figs. S13–S19). These catalysis results suggest that the reaction mechanisms of transfer hydrogenation over Ru-MSP-II are quite similar among these substrates, and the reaction rates are likely decreased by the steric hindrance effect. Apart from the steric hindrance effect, it is reported that electron-denoting substituents such as methyl may increase the electron density of carbon atom in the carbonyl group, which is unfavorable for carbonyl reduction [54]. It is also shown that Ru-MSP-II is catalytically active toward the transfer hydrogenation of furfural into furfuryl alcohol with a high selectivity (Table 2, entry 2), indicative of the potential applications of Ru-MSP-II to upgrade the biomass derivatives through carbonyl reduction. These results demonstrate that the optimized Ru-MSP catalyst in this study (*i.e.*, Ru-MSP-II) is a highly active and selective heterogeneous catalyst that is capable of the transfer hydrogenation of carbonyl compounds using formate. Furthermore, this optimized Ru-MSP catalyst shows desired physicochemical properties including high stability, reusability, and wide scope of substrates, which holds the promise as a practical catalyst for industrial applications.

4. Conclusions

In this study, the ruthenium-based metallo-supramolecular polymer (Ru-MSP) was rationally synthesized as a heterogeneous catalyst for carbonyl reduction through the liquid-phase transfer hydrogenation using formate as the hydrogen donor under ambient conditions. Ru-MSP catalysts were synthesized using 1,4-bis(1,10-phenanthrolin-5-yl)benzene as the pincer ligand to coordinate Ru cations. The degree of polymerization and local environment of Ru atoms of Ru-MSP were controlled by tuning the ligand/metal ratio and the synthesis period/temperature. The coordinatively-unsaturated Ru atoms, *i.e.*, coordinated with only four N atoms of pincer ligand, are found to be the active sites responsible for the selective transfer hydrogenation of benzaldehyde to benzyl alcohol over Ru-MSP catalysts. The prepared Ru-MSP catalyst displays a much higher benzyl alcohol yield than a number of Ru-based materials including heterogeneous Ru/C, homogeneous $RuCl_3$, $Ru(DMSO)_4Cl_2$, and $Ru(phen)_2Cl_2$ (the monomeric analogue of Ru-MSP). Experimental observations and theoretical calculations suggest that such polymerization-induced activity improvement is due to the enhanced electron transfer from ligands to Ru atoms and the increased electrophilicity of ligands, which facilitate the selective dehydrogenation of formate *via* C-H bond dissociation and the activation of carbonyl compounds *via* adsorption of carbonyl oxygen. The synthesized Ru-MSP catalyst exhibits promising heterogeneity, reusability, and capability for catalyzing a wide scope of carbonyl substrates. The findings presented in this work demonstrate that the delicate control of polymerization of metal ions with pincer ligands could yield heterogeneous metal complex catalysts with exceptional performance and desirable reusability, which are more desirable than the conventional immobilization methods.

CRediT authorship contribution statement

Zi-Jie Gong: Conceptualization, Methodology, Investigation, Writing – original draft, Writing – review & editing, Visualization. **Yemineni S. L. V. Narayana:** Methodology, Investigation, Writing – review & editing. **Yen-Chun Lin:** Methodology, Software. **Wei-Hsiang Huang:** Methodology, Investigation. **Wei-Nien Su:** Methodology, Resources, Writing – review & editing. **Yi-Pei Li:** Methodology, Software, Resources, Writing – review & editing. **Masayoshi Higuchi:** Conceptualization, Methodology, Writing – review & editing, Project administration, Funding acquisition. **Wen-Yueh Yu:** Conceptualization, Methodology, Writing – original draft, Writing – review & editing, Visualization, Supervision, Project administration, Funding acquisition.

Declaration of Competing Interest

The authors declare that they have no known competing financial interests or personal relationships that could have appeared to influence the work reported in this paper.

Acknowledgements

This work is financially supported by the Ministry of Science and Technology (MOST) in Taiwan (MOST 107-2218-E-002-029-MY3, 109-2221-E-002-103-MY3, and 110-2923-E-002-005-MY2), and by the "Advanced Research Center for Green Materials Science and Technology" from The Featured Area Research Center Program within the framework of the Higher Education Sprout Project by the Ministry of Education (110L9006) and the MOST in Taiwan (MOST 110-2524-F-002-043). Zi-Jie Gong is grateful for the fellowship from the International Cooperative Graduate Program (ICGP), National Institute for Materials Science (NIMS), Japan. We gratefully thank Ms Huang, Shou-Ling for the assistance in NMR experiments of the Instrumentation Center at NTU which is supported by the Ministry of Science and Technology, Taiwan. The authors thank Dr. Chih-Wen Pao (Beamline 44A) and Dr. Ting-Shan Chan (Beamline 16A) in NSRRC for assisting the XAS measurements, and thank Ms. C.-Y. Chien of Ministry of Science and Technology (National Taiwan University) for the assistance in TEM experiments. Yi-Pei Li is supported by the Einstein Program funded by Taiwan MOST Young Scholar Fellowship (110-2636-E-002-014). We are grateful to the National Center for High-performance Computing and the Computer and Information Networking Center at NTU for the support of computing facilities.

Appendix A. Supporting information

Supplementary data associated with this article can be found in the online version at doi:10.1016/j.apcatb.2022.121383.

References

[1] A.Y. Li, A. Moores, Carbonyl reduction and biomass: a case study of sustainable catalysis, ACS Sustain. Chem. Eng. 7 (2019) 10182–10197, https://doi.org/10.1021/acssuschemeng.9b00811.
[2] R. Padilla, S. Koranchalil, M. Nielsen, Efficient and selective catalytic hydrogenation of furanic aldehydes using well defined Ru and Ir pincer complexes, Green Chem. 22 (2020) 6767–6772, https://doi.org/10.1039/d0gc90140g.
[3] D. Wang, D. Astruc, The golden age of transfer hydrogenation, Chem. Rev. 115 (2015) 6621–6686, https://doi.org/10.1021/acs.chemrev.5b00203.
[4] M.J. Gilkey, B.J. Xu, Heterogeneous catalytic transfer hydrogenation as an effective pathway in biomass upgrading, ACS Catal. 6 (2016) 1420–1436, https://doi.org/10.1021/acscatal.5b02171.
[5] E. Barath, Hydrogen transfer reactions of carbonyls, alkynes, and alkenes with noble metals in the presence of alcohols/ethers and amines as hydrogen donors, Catalysts 8 (2018) 25, https://doi.org/10.3390/catal8120671.
[6] R.F. Nie, Y.W. Tao, Y.Q. Nie, T.L. Lu, J.S. Wang, Y.S. Zhang, X.Y. Lu, C.C. Xu, Recent advances in catalytic transfer hydrogenation with formic acid over heterogeneous transition metal catalysts, ACS Catal. 11 (2021) 1071–1095, https://doi.org/10.1021/acscatal.0c04939.
[7] L. Xu, R.F. Nie, X.L. Lyu, J.C. Wang, X.Y. Lu, Selective hydrogenation of furfural to furfuryl alcohol without external hydrogen over N-doped carbon confined Co catalysts, Fuel Process. Technol. 197 (2020) 8, https://doi.org/10.1016/j.fuproc.2019.106205.
[8] L.H. Gong, Y.Y. Cai, X.H. Li, Y.N. Zhang, J. Su, J.S. Chen, Room-temperature transfer hydrogenation and fast separation of unsaturated compounds over heterogeneous catalysts in an aqueous solution of formic acid, Green. Chem. 16 (2014) 3746–3751, https://doi.org/10.1039/c4gc00981a.
[9] J. Mondal, Q.T. Trinh, A. Jana, W.K.H. Ng, P. Borah, H. Hirao, Y.L. Zhao, Size-dependent catalytic activity of palladium nanoparticles fabricated in porous organic polymers for alkene hydrogenation at room temperature, ACS Appl. Mater. Interfaces 8 (2016) 15307–15319, https://doi.org/10.1021/acsami.6b03127.
[10] Y.J. Chou, H.C. Ku, C.C. Chien, C.C. Hu, W.Y. Yu, Palladium nanoparticles supported on nanosheet-like graphitic carbon nitride for catalytic transfer hydrogenation reaction, Catal. Sci. Technol. 10 (2020) 7883–7893, https://doi.org/10.1039/dOcy01703e.
[11] A.M. Palvolgyi, J. Bitai, V. Zeindlhofer, C. Schroder, K. Bica, Ion-tagged chiral ligands for asymmetric transfer hydrogenations in aqueous medium, ACS Sustain. Chem. Eng. 7 (2019) 3414–3423, https://doi.org/10.1021/acssuschemeng.8b05613.
[12] Y.W. Wei, D. Xue, Q. Lei, C. Wang, J.L. Xiao, Cyclometalated iridium complexes for transfer hydrogenation of carbonyl groups in water, Green Chem. 15 (2013) 629–634, https://doi.org/10.1039/c2gc36619c.

[13] A.H. Ngo, L.H. Do, Structure-activity relationship study of halfsandwich metal complexes in aqueous transfer hydrogenation catalysis, Inorg. Chem. Front. 7 (2020) 5283–5291, https://doi.org/10.1039/c9qi01310e.
[14] H.A. Younus, N. Ahmad, W. Su, F. Verpoort, Ruthenium pincer complexes: Ligand design and complex synthesis, Coord. Chem. Rev. 276 (2014) 112–152, https://doi.org/10.1016/j.ccr.2014.06.016.
[15] C.Y. Wei, Y. He, X.D. Shi, Z.G. Song, Terpyridine-metal complexes: applications in catalysis and supramolecular chemistry, Coord. Chem. Rev. 385 (2019) 1–19, https://doi.org/10.1016/j.ccr.2019.01.005.
[16] S. Werkmeister, J. Neumann, K. Junge, M. Beller, Pincer-type complexes for catalytic (de)hydrogenation and transfer (de)hydrogenation reactions: recent progress, Chem. Eur. J. 21 (2015) 12226–12250, https://doi.org/10.1002/chem.201500937.
[17] N. End, K.U. Schoning, Immobilized catalysts in industrial research and application, in: A. Kirschning (Ed.), Immobilized Catalysts: Solid Phases, Immobilization and Applications, Springer-Verlag, Berlin, 2004, pp. 241–271, https://doi.org/10.1007/b96878.
[18] P. McMorn, G.J. Hutchings, Heterogeneous enantioselective catalysts: strategies for the immobilisation of homogeneous catalysts, Chem. Soc. Rev. 33 (2004) 108–122, https://doi.org/10.1039/b200387m.
[19] T. Terashima, M. Ouchi, T. Ando, M. Sawamoto, Transfer hydrogenation of ketones catalyzed by PEG-armed ruthenium-microgel star polymers: microgel-core reaction space for active, versatile and recyclable catalysis, Polym. J. 43 (2011) 770–777, https://doi.org/10.1038/pj.2011.52.
[20] B.G.P. van Ravensteijn, D.J. Schild, W.K. Kegel, R.J.M.Klein Gebbink, The immobilization of a transfer hydrogenation catalyst on colloidal particles, ChemCatChem 9 (2017) 440–450, https://doi.org/10.1002/cctc.201601096.
[21] G.M. Eichenseer, B. Kastl, M.A. Pericas, P.R. Hanson, O. Reiser, Synthesis and application of magnetic noyori-type ruthenium catalysts for asymmetric transfer hydrogenation reactions in water, ACS Sustain. Chem. Eng. 4 (2016) 2698–2705, https://doi.org/10.1021/acssuschemeng.6b00197.
[22] P.J. Tseng, C.L. Chang, Y.H. Chan, L.Y. Ting, P.Y. Chen, C.H. Liao, M.L. Tsai, H. H. Chou, Design and synthesis of cycloplatinated polymer dots as photocatalysts for visible-light-driven hydrogen evolution, ACS Catal. 8 (2018) 7766–7772, https://doi.org/10.1021/acscatal.8b01678.
[23] Z.Z. Gao, Y.Y. Xu, Z.K. Wang, H. Wang, D.W. Zhang, Z.T. Li, Porous Ru(bpy)(3) (2+)-cored metallosupramolecular polymers: preparation and recyclable photocatalysis for the formation of amides and 2-diazo-2-phenylacetates, ACS Appl. Polym. Mater. 2 (2020) 4885–4892, https://doi.org/10.1021/acsapm.0c00800.
[24] A. Winter, U.S. Schubert, Synthesis and characterization of metallo-supramolecular polymers, Chem. Soc. Rev. 45 (2016) 5311–5357, https://doi.org/10.1039/c6cs00182c.
[25] M.K. Bera, Y. Ninomiya, M. Higuchi, Constructing alternated heterobimetallic Fe (II)/Os(II) supramolecular polymers with diverse solubility for facile fabrication of voltage-tunable multicolor electrochromic devices, ACS Appl. Mater. Interfaces 12 (2020) 14376–14385, https://doi.org/10.1021/acsami.9b21966.
[26] M.D. Hossain, C. Chakraborty, U. Rana, S. Mondal, H.J. Holdt, M. Higuchi, Green-to-black electrochromic copper(I)-based metallo-supramolecular polymer with a perpendicularly twisted structure, ACS Appl. Polym. Mater. 2 (2020) 4449–4454, https://doi.org/10.1021/acsapm.0c00559.
[27] M.D. Hossain, M. Higuchi, Synthesis of metallo-supramolecular polymers using 5,5 '-linked bis(1,10-phenanthroline) ligands, Synthesis 45 (2013) 753–758, https://doi.org/10.1055/s-0032-1316858.
[28] K. Hara, H. Sugihara, L.P. Singh, A. Islam, R. Katoh, M. Yanagida, K. Sayama, S. Murata, H. Arakawa, New Ru(II) phenanthroline complex photo sensitizers having different number of carboxyl groups for dye-sensitized solar cells, J. Photochem. Photobiol. Chem. 145 (2001) 117–122, https://doi.org/10.1016/s1010-6030(01)00570-6.
[29] J. Gopinath, K.H. Park, S.J. Kim, V. Santosh, A.V.S. Sainath, M. Dhayal, Phenanthroline-based ruthenium complexes for enhanced charge transportation in solvent-free ionic liquid electrolyte, J. Mater. Sci. 52 (2017) 10545–10556, https://doi.org/10.1007/s10853-017-1207-2.
[30] Y.S.L.V. Narayana, C. Chakraborty, U. Rana, Y. Ninomiya, T. Yoshida, M. Higuchi, Modulation of a coordination structure in a europium(III)-based metallo-supramolecular polymer for high proton conduction, RSC Adv. 8 (2018) 37193–37199, https://doi.org/10.1039/c8ra07405d.
[31] M. Baidossi, A.V. Joshi, S. Mukhopadhyay, Y. Sasson, Pd/C-catalyzed transfer-hydrogenation of benzaldehydes to benzyl alcohols using potassium formate as the selective hydrogen donor, Synth. Commun. 34 (2004) 643–650, https://doi.org/10.1081/scc-120027711.
[32] Y.X. Gao, S. Jaenicke, G.K. Chuah, Highly efficient transfer hydrogenation of aldehydes and ketones using potassium formate over AlO(OH)-entrapped ruthenium catalysts, Appl. Catal. A Gen. 484 (2014) 51–58, https://doi.org/10.1016/j.apcata.2014.07.010.
[33] I. Szatmari, G. Papp, F. Joo, A. Katho, Unexpectedly fast catalytic transfer hydrogenation of aldehydes by formate in 2-propanol-water mixtures under mild conditions, Catal. Today 247 (2015) 14–19, https://doi.org/10.1016/j.cattod.2014.06.023.
[34] A.D. Becke, Density-functional thermochemistry.3. The role of exact exchange, J. Chem. Phys. 98 (1993) 5648–5652, https://doi.org/10.1063/1.464913.
[35] P.J. Stephens, F.J. Devlin, C.F. Chabalowski, M.J. Frisch, Ab-initio calculation of vibrational absorption and circular-dichroism spectra using density-functional force-fields, J. Phys. Chem. 98 (1994) 11623–11627, https://doi.org/10.1021/j100096a001.
[36] F. Weigend, R. Ahlrichs, Balanced basis sets of split valence, triple zeta valence and quadruple zeta valence quality for H to Rn: design and assessment of accuracy, Phys. Chem. Chem. Phys. 7 (2005) 3297–3305, https://doi.org/10.1039/b508541a.
[37] E. Epifanovsky, A.T.B. Gilbert, X.T. Feng, J. Lee, Y.Z. Mao, N. Mardirossian, P. Pokhilko, A.F. White, M.P. Coons, A.L. Dempwolff, Z.T. Gan, D. Hait, P.R. Horn, L.D. Jacobson, I. Kaliman, J. Kussmann, A.W. Lange, K.U. Lao, D.S. Levine, J. Liu, S.C. McKenzie, A.F. Morrison, K.D. Nanda, F. Plasser, D.R. Rehn, M.L. Vidal, Z. Q. You, Y. Zhu, B. Alam, B.J. Albrecht, A. Aldossary, E. Alguire, J.H. Andersen, V. Athavale, D. Barton, K. Begam, A. Behn, N. Bellonzi, Y.A. Bernard, E.J. Berquist, H.G.A. Burton, A. Carreras, K. Carter-Fenk, R. Chakraborty, A.D. Chien, K. D. Closser, V. Cofer-Shabica, S. Dasgupta, M. de Wergifosse, J. Deng, M. Diedenhofen, H. Do, S. Ehlert, P.T. Fang, S. Fatehi, Q.G. Feng, T. Friedhoff, J. Gayvert, Q.H. Ge, G. Gidofalvi, M. Goldey, J. Gomes, C.E. Gonzalez-Espinoza, S. Gulania, A.O. Gunina, M.W.D. Hanson-Heine, P.H.P. Harbach, A. Hauser, M. F. Herbst, M.H. Vera, M. Hodecker, Z.C. Holden, S. Houck, X.K. Huang, K. Hui, B. C. Huynh, M. Ivanov, A. Jasz, H. Ji, H.J. Jiang, B. Kaduk, S. Kahler, K. Khistyaev, J. Kim, G. Kis, P. Klunzinger, Z. Koczor-Benda, J.H. Koh, D. Kosenkov, L. Koulias, T. Kowalczyk, C.M. Krauter, K. Kue, A. Kunitsa, T. Kus, I. Ladjanszki, A. Landau, K. V. Lawler, D. Lefrancois, S. Lehtola, R.R. Li, Y.P. Li, J.S. Liang, M. Liebenthal, H. H. Lin, Y.S. Lin, F.L. Liu, K.Y. Liu, M. Loipersberger, A. Luenser, A. Manjanath, P. Manohar, E. Mansoor, S.F. Manzer, S.P. Mao, A.V. Marenich, T. Markovich, S. Mason, S.A. Maurer, P.F. McLaughlin, M. Menger, J.M. Mewes, S.A. Mewes, P. Morgante, J.W. Mullinax, K.J. Oosterbaan, G. Paran, A.C. Paul, S.K. Paul, F. Pavosevic, Z. Pei, S. Prager, E.I. Proynov, A. Rak, E. Ramos-Cordoba, B. Rana, A. E. Rask, A. Rettig, R.M. Richard, F. Rob, E. Rossomme, T. Scheele, M. Scheurer, M. Schneider, N. Sergueev, S.M. Sharada, W. Skomorowski, D.W. Small, C.J. Stein, Y.C. Su, E.J. Sundstrom, Z. Tao, J. Thirman, G.J. Tornai, T. Tsuchimochi, N. M. Tubman, S.P. Veccham, O. Vydrov, J. Wenzel, J. Witte, A. Yamada, K. Yao, S. Yeganeh, S.R. Yost, A. Zech, I.Y. Zhang, X. Zhang, Y. Zhang, D. Zuev, A. Aspuru-Guzik, A.T. Bell, N.A. Besley, K.B. Bravaya, B.R. Brooks, D. Casanova, J.D. Chai, S. Coriani, C.J. Cramer, G. Cserey, A.E. DePrince, R.A. DiStasio, A. Dreuw, B. D. Dunietz, T.R. Furlani, W.A. Goddard, S. Hammes-Schiffer, T. Head-Gordon, W. J. Hehre, C.P. Hsu, T.C. Jagau, Y.S. Jung, A. Klamt, J. Kong, D.S. Lambrecht, W. Z. Liang, N.J. Mayhall, C.W. McCurdy, J.B. Neaton, C. Ochsenfeld, J.A. Parkhill, R. Peverati, V.A. Rassolov, Y.H. Shao, L.V. Slipchenko, T. Stauch, R.P. Steele, J. E. Subotnik, A.J.W. Thom, A. Tkatchenko, D.G. Truhlar, T. Van Voorhis, T. A. Wesolowski, K.B. Whaley, H.L. Woodcock, P.M. Zimmerman, S. Faraji, P.M. W. Gill, M. Head-Gordon, J.M. Herbert, A.I. Krylov, Software for the frontiers of quantum chemistry: An overview of developments in the Q-Chem 5 package, J. Chem. Phys. 155 (2021) 59, https://doi.org/10.1063/5.0055522.
[38] E.G. Glendening, J.K. Badenhoop, A.E. Reed, J.E. Carpenter, J.A. Bohmann, C.M. Morales, P. Karafiloglou, C.R. Landis, F. Weinhold, NBO 7.0, Theoretical Chemistry Institute, University of Wisconsin, Madison, 2018.
[39] F. Heinemann, J. Karges, G. Gasser, Critical overview of the use of Ru(II) polypyridyl complexes as photosensitizers in one-photon and two-photon photodynamic therapy, Acc. Chem. Res. 50 (2017) 2727–2736, https://doi.org/10.1021/acs.accounts.7b00180.
[40] F.S. Han, M. Higuchi, D.G. Kurth, Metallosupramolecular polyelectrolytes self-assembled from various pyridine ring-substituted bisterpyridines and metal ions: Photophysical, electrochemical, and electrochromic properties, J. Am. Chem. Soc. 130 (2008) 2073–2081, https://doi.org/10.1021/ja710380a.
[41] S. Roeser, F. Bozoglian, C.J. Richmond, A.B. League, M.Z. Ertem, L. Francas, P. Miro, J. Benet-Buchholz, C.J. Cramer, A. Llobet, Water oxidation catalysis with ligand substituted Ru-bpp type complexes, Catal. Sci. Technol. 6 (2016) 5088–5101, https://doi.org/10.1039/c6cy00197a.
[42] O. Impert, A. Kozakiewicz, G. Wrzeszcz, A. Katafias, A. Bienko, R. van Eldik, A. Ozarowski, Characterization of a mixed-valence Ru(II)/Ru(III) ion-pair complex. Unexpected high-frequency electron paramagnetic resonance evidence for Ru(III)-Ru(III) dimer coupling, Inorg. Chem. 59 (2020) 8609–8619, https://doi.org/10.1021/acs.inorgchem.0c01068.
[43] V. Huntosova, S. Gay, P. Nowak-Sliwinska, S.K. Rajendran, M. Zellweger, H. van den Bergh, G. Wagnieres, In vivo measurement of tissue oxygenation by time-resolved luminescence spectroscopy: advantageous properties of dichlorotris(1, 10-phenanthroline)-ruthenium(II) hydrate, J. Biomed. Opt. 19 (2014) 12, https://doi.org/10.1117/1.jbo.19.7.077004.
[44] Y. Pushkar, D. Moonshiram, V. Purohit, L.F. Yan, I. Alperovich, Spectroscopic analysis of catalytic water oxidation by Ru-II(bpy)(tpy)H2O)(2+) suggests that Ru-V$\overline{\text{O}}$O is not a rate-limiting intermediate, J. Am. Chem. Soc. 136 (2014) 11938–11945, https://doi.org/10.1021/ja506586b.
[45] I. Arcon, A. Bencan, A. Kodre, M. Kosec, X-ray absorption spectroscopy analysis of Ru in La_2RuO_5, X Ray Spectrom. 36 (2007) 301–304, https://doi.org/10.1002/xrs.946.
[46] C. Milsmann, E. Bill, T. Weyhermuller, S.D. George, K. Wieghardt, Electronic structures of Ru-II(cyclam)(Et(2)dtc) (+), Ru(cyclam)(tdt) (+), and Ru(cyclam)(tdt) (2+): An X-ray absorption spectroscopic and computational study (tdt = toluene-3,4-dithiolate; Et(2)dtc = N,N-diethyldithiocarbamate(1-)), Inorg. Chem. 48 (2009) 9754–9766, https://doi.org/10.1021/ic9011845.
[47] M.A. Hoque, M. Gil-Sepulcre, A. de Aguirre, J. Elemans, D. Moonshiram, R. Matheu, Y.Y. Shi, J. Benet-Buchholz, X. Sala, M. Malfois, E. Solano, J. Lim, A. Garzon-Manjon, C. Scheu, M.R. Lanza, F. Maseras, C. Gimbert-Surinach, A. Llobet, Water oxidation electrocatalysis using ruthenium coordination oligomers adsorbed on multiwalled carbon nanotubes, Nat. Chem. 12 (2020) 1060–1066, https://doi.org/10.1038/s41557-020-0548-7.
[48] L. Salassa, T. Ruiu, C. Garino, A.M. Pizarro, F. Bardelli, D. Gianolio, A. Westendorf, P.J. Bednarski, C. Lamberti, R. Gobetto, P.J. Sadler, EXAFS, DFT, light-Induced

nucleobase binding, and cytotoxicity of the photoactive complex cis- Ru(bpy)(2)(CO)Cl (+), Organometallics 29 (2010) 6703–6710, https://doi.org/10.1021/om100734y.
[49] S. Muratsugu, M.H. Lim, T. Itoh, W. Thumrongpatanaraks, M. Kondo, S. Masaoka, T.S.A. Hor, M. Tada, Dispersed Ru nanoclusters transformed from a grafted trinuclear Ru complex on SiO_2 for selective alcohol oxidation, Dalton Trans. 42 (2013) 12611–12619, https://doi.org/10.1039/c3dt51142a.
[50] X.J. Cui, W. Li, P. Ryabchuk, K. Junge, M. Beller, Bridging homogeneous and heterogeneous catalysis by heterogeneous single-metal-site catalysts, Nat. Catal. 1 (2018) 385–397, https://doi.org/10.1038/s41929-018-0090-9.
[51] Z.L. Wang, S.M. Xu, Y.Q. Xu, L. Tan, X. Wang, Y.F. Zhao, H.H. Duan, Y.F. Song, Single Ru atoms with precise coordination on a monolayer layered double hydroxide for efficient electrooxidation catalysis, Chem. Sci. 10 (2019) 378–384, https://doi.org/10.1039/c8sc04480e.
[52] A. Blazevic, A.A. Hummer, P. Heffeter, W. Berger, M. Filipits, G. Cibin, B. K. Keppler, A. Rompel, Electronic state of sodium trans- tetrachloridobis(1H-indazole)ruthenate(III) (NKP-1339) in tumor, liver and kidney tissue of a SW480-bearing mouse, Sci. Rep. 7 (2017) 8, https://doi.org/10.1038/srep40966.
[53] U. Kokcam-Demir, A. Goldman, L. Esrafili, M. Gharib, A. Morsali, O. Weingart, C. Janiak, Coordinatively unsaturated metal sites (open metal sites) in metal-organic frameworks: design and applications, Chem. Soc. Rev. 49 (2020) 2751–2798, https://doi.org/10.1039/c9cs00609e.
[54] A.H. Valekar, M. Lee, J.W. Yoon, J. Kwak, D.Y. Hong, K.R. Oh, G.Y. Cha, Y. U. Kwon, J. Jung, J.S. Chang, Y.K. Hwang, Catalytic transfer hydrogenation of furfural to furfuryl alcohol under mild conditions over Zr-MOFs: Exploring the role of metal node coordination and modification, ACS Catal. 10 (2020) 3720–3732, https://doi.org/10.1021/acscatal.9b05085.
[55] K. Mori, M. Dojo, H. Yamashita, Pd and Pd-Ag nanoparticles within a macroreticular basic resin: An efficient catalyst for hydrogen production from formic acid decomposition, ACS Catal. 3 (2013) 1114–1119, https://doi.org/10.1021/cs400148n.
[56] Q.Y. Bi, J.D. Lin, Y.M. Liu, H.Y. He, F.Q. Huang, Y. Cao, Dehydrogenation of formic acid at room temperature: boosting palladium nanoparticle efficiency by coupling with pyridinic-nitrogen-doped carbon, Angew. Chem. Int. Ed. 55 (2016) 11849–11853, https://doi.org/10.1002/anie.201605961.
[57] M. Naulani-Garcia, D. Salinas-Torres, K. Mori, Y. Kuwahara, H. Yamashita, Enhanced formic acid dehydrogenation by the synergistic alloying effect of PdCo catalysts supported on graphitic carbon nitride, Int. J. Hydrog. Energy 44 (2019) 28483–28493, https://doi.org/10.1016/j.ijhydene.2018.11.057.
[58] K. Tedsree, T. Li, S. Jones, C.W.A. Chan, K.M.K. Yu, P.A.J. Bagot, E.A. Marquis, G. D.W. Smith, S.C.E. Tsang, Hydrogen production from formic acid decomposition at room temperature using a Ag-Pd core-shell nanocatalyst, Nat. Nanotechnol. 6 (2011) 302–307, https://doi.org/10.1038/nnano.2011.42.
[59] A. Iida, A. Sekioka, S. Yamaguchi, Heteroarene-fused boroles: what governs the antiaromaticity and Lewis acidity of the borole skeleton? Chem. Sci. 3 (2012) 1461–1466, https://doi.org/10.1039/c2sc20100c.
[60] J.L. Zhou, L.L. Liu, L.L. Cao, D.W. Stephan, Nitrogen-based lewis acids: synthesis and reactivity of a cyclic (alkyl)(amino)nitrenium cation, Angew. Chem. Int. Ed. 57 (2018) 3322, https://doi.org/10.1002/anie.201713118.
[61] A. Maity, T.S. Teets, Main group Lewis acid-mediated transformations of transition-metal hydride complexes, Chem. Rev. 116 (2016) 8873–8911, https://doi.org/10.1021/acs.chemrev.6b00034.
[62] K. Nakajima, M. Tominaga, M. Waseda, H. Miura, T. Shishido, Highly efficient supported palladium-gold alloy catalysts for hydrogen storage based on ammonium bicarbonate/formate redox cycle, ACS Sustain. Chem. Eng. 7 (2019) 6522–6530, https://doi.org/10.1021/acssuschemeng.8b04698.
[63] D.Y. Shin, M.S. Kim, J.A. Kwon, Y.J. Shin, C.W. Yoon, D.H. Lim, Fundamental mechanisms of reversible dehydrogenation of formate on N-doped graphene-supported Pd nanoparticles, J. Phys. Chem. C 123 (2019) 1539–1549, https://doi.org/10.1021/acs.jpcc.8b07002.
[64] S. Masuda, Y. Shimoji, K. Mori, Y. Kuwahara, H. Yamashita, Interconversion of formate/bicarbonate for hydrogen storage/release: Improved activity following sacrificial surface modification of a $Ag@Pd/TiO_2$ catalyst with a TiO_x Shell, ACS Appl. Energy Mater. 3 (2020) 5819–5829, https://doi.org/10.1021/acsaem.0c00744.
[65] X.D. Li, P. Jia, T.F. Wang, Furfural: A promising platform compound for sustainable production of C-4 and C-5 chemicals, ACS Catal. 6 (2016) 7621–7640, https://doi.org/10.1021/acscatal.6b01838.